

Single π^- production in np collisions for excess energies up to 90 MeV

COSY-TOF collaboration

M. Abdel-Bary^d, K.-Th. Brinkmann^a, H. Clement^c, E. Doroshkevich^c, S. Dshemuchadse^a, A. Erhardt^c, W. Eyrich^b, H. Freiesleben^a, A. Gillitzer^d, R. Jäkel^a, L. Karsch^a, K. Kilian^d, E. Kuhlmann^{a,#}, K. Möller^e, H.P. Morsch^{d,f}, L. Naumann^e, N. Paul^d, C. Pizzolotto^b, J. Ritman^d, E. Roderburg^d, W. Schroeder^b, M. Schulte-Wissermann^a, Th. Sefzick^d, A. Teufel^b, A. Ucar^d, P. Wintz^d, P. Wüstner^d, and P. Zupranski^f

^a Institut für Kern- und Teilchenphysik, Technische Universität Dresden, D-01062 Dresden, Germany

^b Physikalisches Institut, Universität Erlangen, D-91058 Erlangen, Germany

^c Physikalisches Institut, Universität Tübingen, D-72076 Tübingen, Germany

^d Institut für Kernphysik, Forschungszentrum Jülich, D-52425 Jülich, Germany

^e Institut für Strahlenphysik, Forschungszentrum Dresden-Rossendorf, D-01314 Dresden, Germany

^f Andrzej Soltan Institute for Nuclear Studies, PL-00681, Warsaw, Poland

August 15, 2007

Abstract The quasifree reaction $np \rightarrow pp\pi^-$ was studied in a kinematically complete experiment by bombarding a liquid hydrogen target with a deuteron beam of momentum 1.85 GeV/c and analyzing the data along the lines of the spectator model. In addition to the three charged ejectiles the spectator proton was also detected in the large-acceptance time-of-flight spectrometer COSY-TOF. It was identified by its momentum and flight direction thus yielding access to the Fermi motion of the bound neutron and to the effective neutron 4-momentum vector \mathbb{P}_n which differed from event to event. A range of almost 90 MeV excess energy above threshold was covered. Energy dependent angular distributions, invariant mass spectra as well as fully covered Dalitz plots were deduced. Sizeable pp FSI effects were found as were contributions of p and d partial waves. The behavior of the elementary cross section σ_{01} close to threshold is discussed in view of new cross section data. In comparison with existing literature data the results provide a sensitive test of the spectator model.

PACS numbers: 13.75.Cs, 25.10.+s, 29.20.Dh

corresponding author, e-mail: e.kuhlmann@physik.tu-dresden.de

1 Introduction

The low-energy regime in strong interaction physics is known to be dominated by pion producing reactions. Pioneering experiments were first carried out with bubble chambers which somewhat later were superseded by more refined experiments with electronic detectors at such hadron facilities as TRIUMF, LAMPF, PSI, and SATURNE and then, starting in the late 1980s, at the cooler rings IUCF, CELSIUS, and COSY. A vast amount of data on meson production in general and on pion production in particular became available, as can be seen in the recent review articles from the experimental [1] and the theoretical side [2]. Assuming isospin invariance, all single pion production reactions in NN collisions with three body final states can be decomposed into a sum of at most two out of three elementary cross sections σ_{I_i, I_f} [3] with I_i and I_f denoting the isospin of the NN system in the initial and final state, respectively. Starting from the pp -entrance channel two reactions are possible, $pp \rightarrow pp\pi^0$ and $pp \rightarrow pn\pi^+$, yielding, respectively, σ_{11} and $\sigma_{11} + \sigma_{10}$. The isoscalar cross section σ_{01} can only be determined in neutron-proton collisions as, *e.g.*, $\sigma_{np \rightarrow pp\pi^-} = \frac{1}{2}(\sigma_{11} + \sigma_{01})$ and hence

$$\sigma_{01} = 2 \cdot \sigma_{np \rightarrow pp\pi^-} - \sigma_{pp \rightarrow pp\pi^0}. \quad (1)$$

Close to threshold only a few partial waves have to be considered. In a simple, semiclassical picture the maximum $l = l_{max}$ is given by $l_{max} \simeq R \cdot q$. Here R , which gives the distance from the center of the NN collision where a pion of momentum q is created, is of order $h/(m_\pi c)$, *i.e.*, the compton wavelength of the pion, and hence $l_{max} \simeq q/m_\pi \simeq \eta$. This dimensionless parameter η is often found in the literature for specifying excess above threshold. A more direct measure is the excess energy $Q = \sqrt{s} - \sqrt{s_0}$ with $\sqrt{s}(\sqrt{s_0})$ denoting the total CM energy (the threshold energy), respectively. Since for excess energies less than 100 MeV η is well below 1.5, only partial waves of type Ss, Sp, Ps and Pp as, *e.g.*, ${}^3P_0 \rightarrow {}^1S_0 s_0$ have to be considered, whereas the role of $l = 2$ contributions (Sd and Ds) can be regarded as negligible. Here the Rosenfeld notation $L_p l_q$ has been used [3] with L_p being the orbital angular momentum of the NN pair, l_q that of the pion with respect to this pair.

In the past the pp entrance channel attracted most of the attention. Only recently the focus was shifted to a larger degree towards the study of proton-neutron collisions. In this case one might either use a neutron beam impinging on a hydrogen target or use a deuterium target as a substitute for a neutron and use the spectator model to determine the observables of the quasifree reaction. The former approach was extensively used by the Freiburg group

working at PSI [4-7] and to some extent by groups at LAMPF [8] and TRIUMF [9]. The first dedicated experiments on a deuterium target were also performed at TRIUMF [10,11] where in order to bypass the difficulties of low-energy spectator detection, the final-state protons were restricted to the 1S_0 , the “diproton” state, by selecting only two-proton events with a small relative momentum. Alternatively one can use a deuteron beam hitting a hydrogen target. The advantage of having fast spectator protons flying in the forward direction is counterbalanced by the fact that appropriate deuteron beams beyond 4 GeV/c are not available any more and thus one is restricted to reactions where only light mesons are produced. The feasibility of this approach was investigated in our recent paper [12] on the $dp \rightarrow ppp\pi^-$ reaction.

It is the aim of the present paper on the quasifree $np \rightarrow pp\pi^-$ reaction to present angular distributions, Dalitz plots and invariant mass distributions for the three reaction products, from which one might deduce clues as to the participating partial waves. We will present our data for angles as defined in Fig. 1. In the 3-particle center-of-mass (CM) system all three momentum vectors lie in a plane, their sum adds up to zero. Observables when given in the CM system will be marked with an asterisk. Denoting the beam direction by \vec{N} , the pion momentum by \vec{q}^* and the two proton momenta by \vec{p}_i^* , we will present angular distributions in the two angles $\cos \theta_q^* = \cos(\vec{q}^*, \vec{N})$ and $\cos \theta_P^* = \cos(\vec{P}^*, \vec{N})$ where \vec{P}^* , the relative proton momentum, is taken as the difference vector $\vec{p}_2^* - \vec{p}_1^*$. By construction the latter is symmetric around $\cos \theta_P^* = 0$. Strong interference effects between outgoing Ss and Sp on one hand and Ps and Pp waves on the other will produce highly asymmetric distributions in $\cos \theta_q^*$ even at the lowest $Q(<20 \text{ MeV})$.

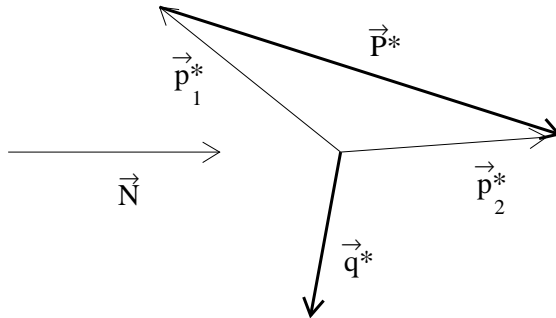


Figure 1: *Definition of the relevant momentum vectors in the CM system.*

2 Experimental Procedure

2.1 Principle of measurement and spectator tagging

The reaction under study is $np \rightarrow pp\pi^-$. Due to the lack of a neutron beam, deuterons were used instead and the data were analyzed along the lines of the spectator model. This method has been described in detail in [12], hence we will give only some short remarks here. The basic idea of the model is that 1) the proton in the deuteron can be regarded as an unaffected spectator staying on-shell throughout the reaction and 2) the matrix element for quasi-free pion production from a bound neutron is identical to that for free pion production from an unbound neutron. Crucial to the method is the task to detect and identify the spectator proton p_s , since the information gathered from this particle gives a direct measure of the Fermi momentum carried by the off-shell neutron within the deuteron at the time of the np reaction. The Fermi momentum distribution as calculated from any of the existing NN potentials has a maximum near 40 MeV/c and a tail extending towards several hundred MeV/c, hence a wide range in excess energy Q can be covered with a monoenergetic deuteron beam. The main result of our recent study was that the two assumptions quoted above can be regarded as being fulfilled for Fermi momenta below 150 MeV/c.

The experiment was carried out with the time-of-flight spectrometer COSY-TOF set up on an external beamline of the proton synchrotron COSY [13] at the Forschungszentrum Jülich. A deuteron beam of momentum $p_d = 1.85$ GeV/c was focussed onto a liquid hydrogen target, charged particles emerging from the reaction zone were detected in a multi-layer scintillator hodoscope with its main components Quirl, Ring and Barrel. Details of the various subdetectors, their performance as well as the different steps necessary for calibrating the whole system have been described in a series of papers, see [12] and references therein. Here only a short overview will be given. By measuring each particle's flight time and direction, their velocity vectors given as $\vec{v} = (\beta, \theta, \phi)$ could be determined with a time-of-flight resolution of better than 300 ps (σ) and an angular track resolution of better than $0.3^\circ(\sigma)$. The momentum 4-vectors \mathbb{P} of all detected particles were then obtained from the measured observables by applying additional mass hypotheses. Carrying out various tests as, *e.g.*, momentum conservation, missing mass and invariant mass analyses as well as comparisons with results obtained from our Monte Carlo simulations helped to find the correct assignment for each event with a high degree of probability as quantified below.

In the reaction $dp \rightarrow pp\pi^- p_s$ four charged particles are emitted which in most cases all are

detected in the time-of-flight spectrometer. Thus the main trigger condition was such that a total of four hits was required in any of the stop scintillator hodoscopes Quirl, Ring and Barrel and at least one hit in the twelve-fold segmented start scintillator. Due to the fact that pions can also be emitted into the backward region where no detector was installed we set up a second trigger condition with only three required hits at a reduction factor of 10. Since for these events the unobserved pion can be reconstructed through a missing mass analysis, the full kinematically allowed phase space was covered.

With a beam momentum below the threshold for 2π -production, any 4-hit event apart from accidentals could only result from the reaction under study. As the first step in our analysis we checked on the four possible hypotheses, *i.e.*, the pion being particle 1, 2, 3, or 4 and calculated for each case the sums of longitudinal and transversal momentum components $\sum p_L$ and $\sum p_T$. As the correct assignment we took the one where these values were closest to $\sum p_L = p_d$ and $\sum p_T = 0$. As the spectator proton we then chose the one which was detected close to the beam axis with a momentum near $p_d/2$. The spread in Fermi momentum caused the momentum of the spectator to vary considerably, higher Q values correspond to lower momenta and vice versa. This is illustrated in Fig. 2 where for two narrow ranges in Q ([18.0-34.0] and [61.0-74.5] MeV) the momentum distribution of the spectator proton and the summed distribution of both reaction protons is plotted. The spectator distribution given by the solid histogram at a mean $\langle Q \rangle = 26$ MeV sticks out as a sharp line well separated from the much broader momentum distribution of the other two protons, whereas at $\langle Q \rangle = 68$ MeV the spectator line is still rather narrow, but starts to overlap with the one of the reaction protons. Since a unique identification of the spectator is essential for the analysis we found it necessary to also limit the range in Q due to this effect and only considered events where the excess energy was below 90 MeV which roughly coincides with our proposed limit for the Fermi momentum [12]. In our finally accepted data sample of $2.2 \cdot 10^5$ events we obtained a longitudinal momentum distribution $\sum p_L$ which had its center at p_d with a width of 39 MeV/c (σ). In case of the transversal distribution the spread was even smaller, namely 13 MeV/c. Alternatively we also used the missing mass method for identifying the various ejectiles, see ref.[12], and found full agreement.

Reconstructing those events where the pions were emitted into the backward region by missing mass techniques in principle caused no problems. In several cases, however, we found events where three protons were detected as for a true $dp \rightarrow pp\pi^-p_s$ reaction, only there a third proton was produced in a chain of two consecutive np elastic scattering processes. From the first quasielastic scattering reaction one gets a scattered proton, a forward flying

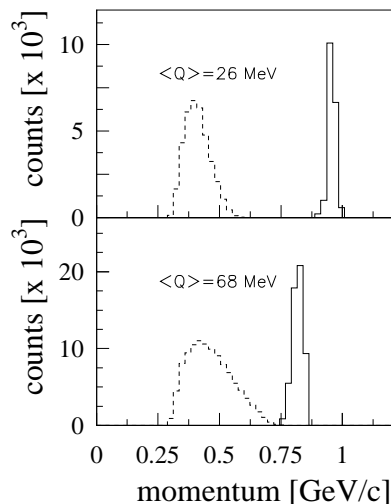


Figure 2: *Experimentally deduced momentum distributions for the spectator protons (solid histograms) and the reaction protons (dashed histograms) for two ranges in Q .*

spectator and a neutron. The scattered neutron in traversing one of the start detector elements hits another proton which reaches the detector whereas the slowed-down neutron remains unobserved. In simulating this process we found that by suitable selections in missing mass and angles these events could be eliminated. Thus an additional set of roughly $0.6 \cdot 10^5$ reconstructed $pp\pi^-p_s$ events was obtained.

As has been outlined in [12], the timing signals deduced from both ends of the Barrel scintillators not only yield information on the flight times, but also on the hit position of any track passing through the Barrel. Hence an important step in the detector calibration is the fixing of the absolute time offset which was carried out through a comparison with the results obtained for dp elastic scattering. This binary reaction with its unique kinematics and sizeable cross section was repeatedly measured in separate runs with an adjusted trigger condition. As a check of the reliability of the event reconstruction we show in Fig. 3 the deuteron angular distribution (given as histograms) in comparison with older data obtained at a somewhat higher beam momentum (solid dots) [14]. Instead of the deuteron beam momentum of 1.85 GeV/c we quote a value of 0.92 GeV/c ($T_{kin} = 376$ MeV) which corresponds to the inverse reaction for a proton beam hitting a deuterium target at the same \sqrt{s} . The absence of data in the forward region is due to the fact that the corresponding protons were emitted towards angles $> 60^\circ$ which is out of the acceptance of the spectrometer. The overall agreement is very good, the apparent mismatch in the peaking of the forward maximum results from the difference in beam momentum p_p . To eliminate this dependency on p_p we

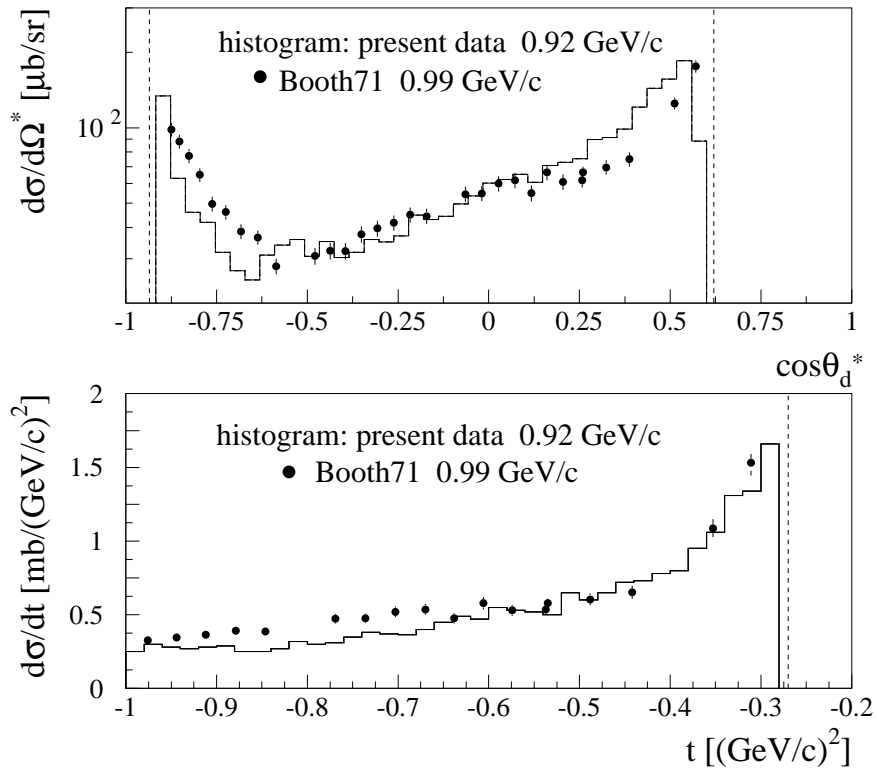


Figure 3: Angular distributions for the elastic pd scattering reaction plotted as a function of the CM angle $\cos\theta_d^*$ (top) and momentum transfer t (bottom) in comparison with data from ref.[14]. The dashed vertical lines denote the acceptance limits of our detector.

plotted the same data (for $\cos\theta_d^* > -0.35$) as a function of the Mandelstam variable t (Fig. 3, lower frame) and found a very satisfying agreement.

2.2 Monte Carlo simulation

The analysis of our experimental data samples was accompanied by extensive Monte Carlo simulations. In order to allow each simulated quasi-free $np \rightarrow pp\pi^-$ -event to have different initial kinematical parameters the program package was modified in a way as was described in detail in [12], hence we will give only a short outline of the main ideas. Using the CERNLIB event generator GENBOD [15] one generates N -body events for a given reaction specified by N , type and mass of the particles involved and the total CM energy \sqrt{s} . The code returns momentum 4-vectors for each ejectile in the overall center-of-mass system and weight factors w_e based on the phase space density of the reaction. In the present case the basic reaction to be simulated is $np \rightarrow pp\pi^-$. For each event randomly chosen values

for $\cos \theta^*$, ϕ^* and momentum $|\vec{p}^*|/(\text{MeV}\cdot\text{c}^{-1})$ were picked, the two former ones following uniform distributions, whereas the momentum was folded with the above mentioned Fermi distribution. We identify the three-component vector $|\vec{p}^*|$, $\cos \theta^*$, ϕ^* as well as the one pointing into the opposite direction with those of an np -pair within the deuteron in its CM system. Transformation into the laboratory system then allows one to deduce the corresponding vectors for spectator and projectile particle within a fast moving deuteron of momentum $p_d = 1.85 \text{ GeV}/c$. The fact that in the laboratory system the flight direction of the projectile neutron deviates by a small angle from that of the beam deuteron is accounted for by a suitably chosen rotation such that the neutron's flight direction serves as the actual beam direction. After having fixed event-by-event the momentum vector for the "beam neutron" it is straightforward to perform the simulation for $np \rightarrow pp\pi^-$.

By using approximately 1 million Monte Carlo events uniformly distributed across the available phase-space we could determine the energy dependent acceptance of our detector and the reconstruction efficiency as a function of excess energy Q . The main limitations in acceptance stemmed from the maximum in detector angle $\theta_{max} = 60^\circ$ and from the charged particles' energy loss in the various detector layers resulting in a low β -threshold of $\beta \approx 0.5$ for π^- mesons and $\beta \approx 0.35$ for protons. In Fig. 4 we show the resulting acceptance curves for the relative proton momentum angle $\cos \theta_P^*$ (left) and the proton-proton invariant mass M_{pp}

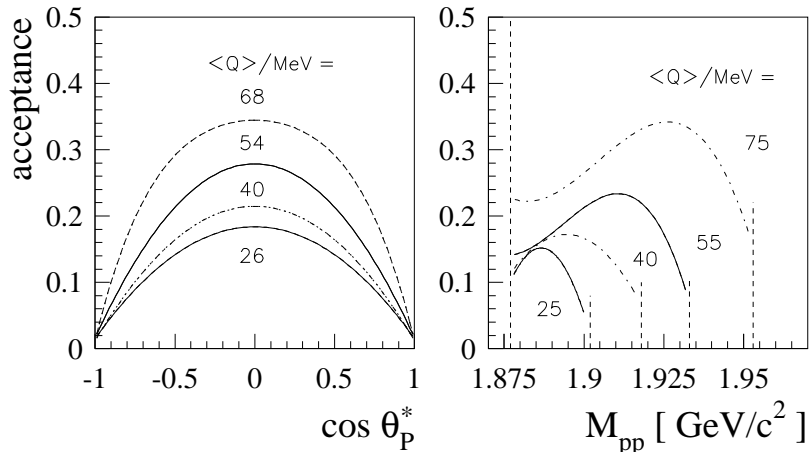


Figure 4: *Simulated acceptance curves as obtained for the relative proton momentum angle $\cos \theta_P^*$ (left) and the proton-proton invariant mass M_{pp} (right) for different values of excess energy Q . The dashed vertical lines in the plot of the right panel denote the kinematical limits.*

M_{pp} (right) for selected values of Q . The acceptance goes to zero near $|\cos \theta_p^*| = 1$. This comes as a result of the way the relative proton momentum vector \vec{P}^* is constructed (see also Fig. 1). When the direction of \vec{P}^* approaches the beam direction, one of the protons in the CM system moves backwards, hence has minimum energy and drops below the detection threshold. Similar calculations have been performed for all other observables.

3 Results and discussion

Cross sections for various emission angles and invariant masses of each two-particle subsystem as well as two-dimensional Dalitz plots were extracted from the data. In order to derive absolute cross sections one must know the integrated luminosity. Defined as $\mathcal{L} = \int n_b \cdot n_t dt$ with $n_b(n_t)$ denoting the number of beam and target particles, respectively, one finds the cross section from the relation

$$\sigma = n / (\mathcal{L} \cdot f \cdot \epsilon), \quad (2)$$

where n is the number of observed events, f the deadtime correction factor and ϵ gives the geometrical and reconstruction efficiency. This simple relation, however, has to be modified in case of a quasifree reaction. The Fermi motion of the neutrons within the deuteron will lead to a wide span in excess energy Q such that the number of beam particles initiating a pn reaction at a given Q will vary. In the present case of a close-to-threshold measurement, one furthermore will observe a strong variation in σ . In order to extract the energy dependence of the cross section and to compare it with the one of the free reaction it is necessary to unfold the effect of the Fermi motion from the data. By dividing the range in Q in small bins $\langle Q \rangle_i$ such that per bin the variation in σ is small and can be approximated by a constant $\bar{\sigma}_i$ the number of produced events N_i is [16]

$$N_i = \bar{\sigma}_i \mathcal{L} \int_{\langle Q \rangle_i} |\phi(p_b)| d^3 \mathbf{p}_b, \quad (3)$$

where the integral is taken over all neutron beam momenta \mathbf{p}_b contributing to $\langle Q \rangle_i$ and $\phi(p_b)$ is the deuteron wave function as given by the PARIS potential [17]. Here \mathcal{L} is again the overall luminosity, its Q -dependence is accounted for by the integral. Correspondingly the number of observed events is given by

$$n_i = N_i \cdot f \cdot \epsilon_i \quad (4)$$

The evaluation of the integral is performed by means of Monte Carlo simulations. Denoting the total number of generated Monte Carlo events by N^{MC} and the one generated for the bin $\langle Q \rangle_i$ by N_i^{MC} the integral is given by the ratio

$$\int_{\langle Q \rangle_i} |\phi(p_b)| d^3 \mathbf{p}_b = \frac{N_i^{MC}}{N^{MC}}. \quad (5)$$

Finally, by using eqs. [3-5] one finds for the cross section

$$\bar{\sigma}_i = \frac{1}{\mathcal{L} \cdot f \cdot \epsilon_i} \cdot \frac{n_i}{N_i^{MC}/N^{MC}}. \quad (6)$$

Defining $\tilde{n}_i = n_i/\epsilon_i$ as the number of observed and acceptance corrected events the cross section is essentially given as $\bar{\sigma}_i \propto \tilde{n}_i/N_i^{MC}$ since \mathcal{L} , f and N^{MC} are constants. This is demonstrated in Fig. 5 where we show the distribution of observed events in the top frame as the solid histogram; it extends from threshold up to 90 MeV. Also shown in this frame is the corresponding distribution as obtained for our Monte Carlo events. Calculated for a deuteron beam momentum of $p_d = 1.85$ GeV/c it has its largest Q values also near 90 MeV, but on the low side starts with a sizeable yield already at threshold. Its maximum is shifted to lower Q values towards the peak of the deuteron wavefunction. When extracting the ratio of the experimentally deduced distribution and the Monte Carlo data, the histogram as shown in the bottom frame is obtained which (note the logarithmic scale) rises by more than two orders of magnitude. Also shown as a dashed curve are the total cross section data obtained with a free neutron beam at PSI [6] and parameterized as a 3rd order polynomial in Q . When applying a suitably chosen normalization factor the present data are in good agreement with these absolute values with only some minor deviations at the lower and upper ends of the covered range. Henceforth this one normalization factor will be used in all of our further presentations and discussions of differential cross sections.

No attempt was made to derive in an independent way absolute cross sections from the present experiment. The natural choice for the determination of the luminosity \mathcal{L} would have been the pd elastic scattering reaction. Although it was quite successfully used for calibration procedures we did not consider it as being suited for finding the size of \mathcal{L} . Firstly the amount of available cross section data is still scarce. Apart from the already mentioned experiment by Booth et al. [14] at $p_p = 0.99$ GeV/c which corresponds to a bombarding energy of 425 MeV we only found one more set of published data by Alder et al. [18] at comparable energies. These authors present data at proton bombarding energies of 316 and 364 MeV covering far backward angles $\cos \theta^* < -0.6$ and at 470 and 590 MeV at angles

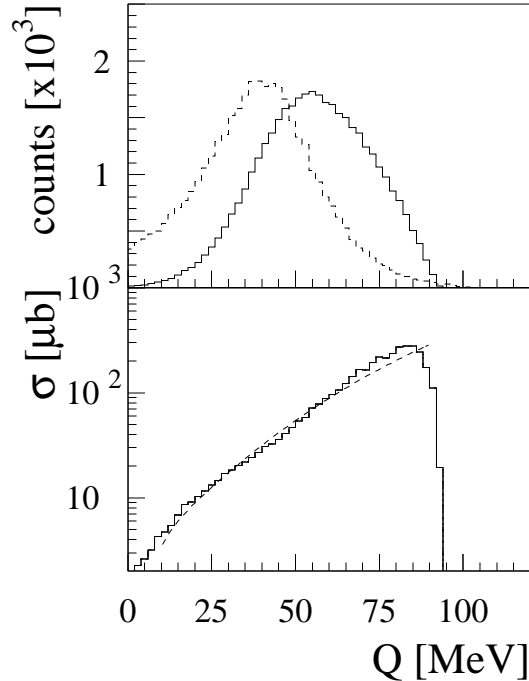


Figure 5: *Top: Simulated (dashed, MC) and measured (solid histogram, exp) distributions of $pp\pi^-$ events as a function of Q . Bottom: Ratio of the two distributions exp/MC (solid histogram) normalized to the cross section data measured at PSI [6] (dashed curve).*

$\cos \theta^* < 0$. Due to this small range in $\cos \theta^*$ we consider these data unfit for a reliable interpolation. Recent data by Gülmez et al. [19] were taken at much higher energies of 641 and 793 MeV, those by Rohdjeß et al. [20] at energies up to 300 MeV. Secondly we found it difficult to estimate the error in σ_{pd} when extracting the dp elastic events from the underlying background which was dominated by the much stronger pp quasielastic scattering events. Finally the uncertainties due to effects like shadowing and rescattering which tend to reduce the cross sections of any quasifree reaction by about 8% [21] and thus add to the size of the systematic error, would only then be of minor consequence when a comparison with another quasifree reaction is carried out.

An order of magnitude estimate of the cross section could nevertheless be made. The integrated luminosity was found from the known target thickness (4 mm liquid hydrogen corresponding to $1.8 \cdot 10^{22}/\text{cm}^2$ target particles), the average beam intensity of $7 \cdot 10^6$ deuterons/s, and the total running time to be of order 40 nb^{-1} . Using eq. 2 with $f \approx 0.5$ and $\epsilon \approx 0.25$ one finds a mean cross section near $60 \mu\text{b}$ in good agreement with the PSI data [6].

3.1 Angular distributions

Acceptance corrected angular distributions are shown in Figs. 6 and 7 together with fits in terms of Legendre polynomials. The excess energy range 1.0-88.0 MeV was cut into six bins, namely [1.0-18.0], [18.0-34.0], [34.0-47.5], [47.5-61.0], [61.0-74.5], and [74.5-88.0] MeV, the indicated excess energies $\langle Q \rangle$ denote the center values of these bins. Error bars when given denote statistical errors only. It should be kept in mind that, although the cross

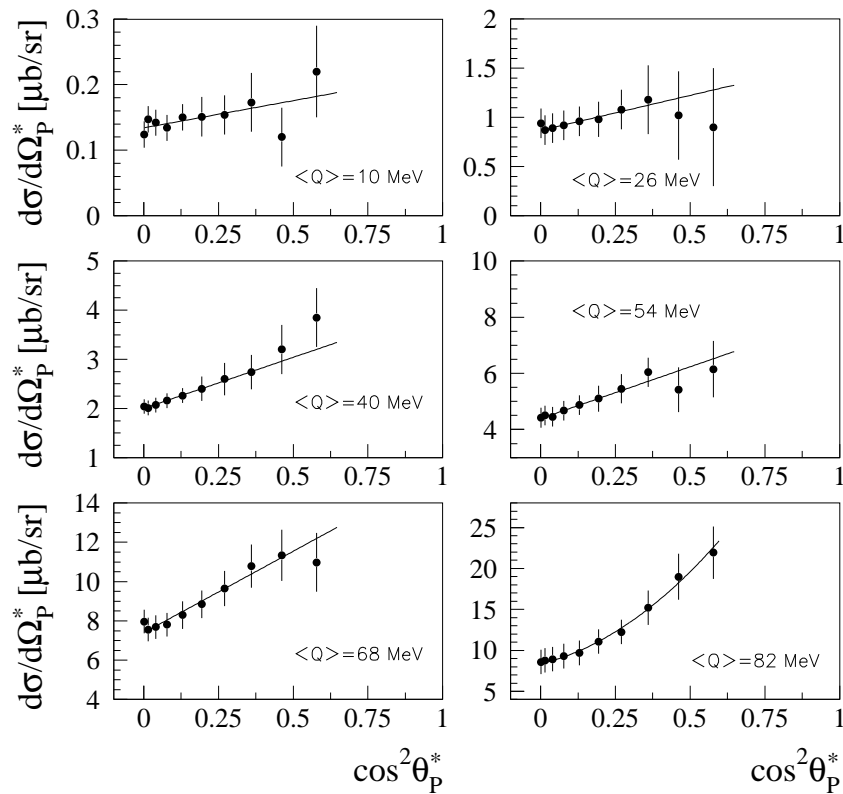


Figure 6: *Angular distributions of the relative proton momentum for selected excess energies $\langle Q \rangle$ together with results of Legendre polynomial fits.*

section rises monotonically with Q , the observed counting rate does not. Due to the non-uniform Fermi distribution which governs the available excess energies, the highest rates are found near $Q = 50$ MeV and consequently one also observes the lowest statistical errors there. As already outlined above (see Fig. 1) the angular distributions of the relative proton momentum by construction are symmetric with respect to $\cos \theta_P^* = 0$. They are plotted as a function of $\cos^2 \theta_P^*$ and were fitted with even Legendre polynomials $W(\cos \theta) \propto 1 + \sum_{\nu} a_{2\nu} \cdot P_{2\nu}(\cos \theta)$ up to $\nu = 2$. The extracted expansion coefficients are given in Table 1, up to

$\langle Q \rangle = 68$ MeV the P_4 -term was neglected. In addition we give the numerical values for $d\sigma/d\Omega^*$ in Table 2 where, as mentioned before, the absolute scale was adjusted to the PSI data [6].

Table 1: *Expansion coefficients of the Legendre polynomial fits to the angular distributions of the relative proton momentum.*

$\langle Q \rangle / \text{MeV}$	a_2	a_4
10	0.34 ± 0.08	-
26	0.43 ± 0.07	-
40	0.51 ± 0.06	-
54	0.44 ± 0.05	-
68	0.54 ± 0.05	-
82	1.28 ± 0.13	0.37 ± 0.13

Table 2: *Differential cross sections in $\mu\text{b}/\text{sr}$ for the angular distributions of the relative proton momentum at six excess energies Q .*

$\cos^2\theta_P^*$	10 MeV	26 MeV	40 MeV	54 MeV	68 MeV	82 MeV
0.002	0.124 ± 0.022	0.94 ± 0.14	2.04 ± 0.16	4.42 ± 0.34	7.96 ± 0.61	8.58 ± 1.31
0.014	0.147 ± 0.023	0.87 ± 0.13	2.01 ± 0.15	4.50 ± 0.36	7.56 ± 0.62	8.78 ± 1.43
0.040	0.142 ± 0.024	0.89 ± 0.15	2.07 ± 0.16	4.45 ± 0.36	7.69 ± 0.64	8.93 ± 1.52
0.078	0.134 ± 0.024	0.92 ± 0.16	2.16 ± 0.17	4.67 ± 0.38	7.81 ± 0.65	9.29 ± 1.48
0.130	0.150 ± 0.024	0.96 ± 0.16	2.26 ± 0.20	4.87 ± 0.38	8.30 ± 0.71	9.70 ± 1.53
0.194	0.151 ± 0.028	0.98 ± 0.16	2.40 ± 0.25	5.10 ± 0.46	8.85 ± 0.73	11.07 ± 1.57
0.270	0.154 ± 0.033	1.08 ± 0.21	2.60 ± 0.33	5.45 ± 0.52	9.65 ± 0.92	12.24 ± 1.60
0.360	0.170 ± 0.044	1.18 ± 0.34	2.74 ± 0.38	6.04 ± 0.54	10.78 ± 1.13	15.21 ± 2.13
0.462	0.120 ± 0.047	1.02 ± 0.46	3.20 ± 0.52	5.42 ± 0.80	11.33 ± 1.31	18.98 ± 2.76
0.578	0.222 ± 0.071	0.90 ± 0.61	3.85 ± 0.63	6.15 ± 1.11	10.98 ± 1.53	21.94 ± 3.12

As one can see from inspection of Fig. 6 the scatter of the data points as well as the size of the error bars increases drastically for values $\cos^2\theta_P^* \geq 0.4$. This is the result of the very low acceptance observed in this angular region (see also the discussion in context with Fig. 4). Accordingly the χ^2 minimisation was only performed on the first eight data points. In the

literature we found one measurement of these proton distributions, which was extracted from roughly 4000 bubble chamber frames [22]. At an average value of Q near 54 MeV the authors report a value of $a_2 = 0.276 \pm 0.032$ which is to be compared to the present one of $a_2 = 0.44 \pm 0.05$. We believe the observed 4σ deviation to be due to systematic errors in their method which were not included in the quoted error. As mentioned above only Ss, Sp, Ps and Pp partial waves should be present in the energy region covered in the present experiment. From our data, however, it can be seen that in the higher Q range contributions of the Ds wave are present as well. Near $\langle Q \rangle = 82$ MeV a $P_4(\cos \theta)$ term with a sizeable expansion coefficient $a_4 = 0.37 \pm 0.13$ had to be included in the fit.

The pion angular distributions as deduced for the same intervals in Q are shown in Fig. 7. In general all are asymmetric and were fitted with sizeable a_1 and a_2 coefficients (see Table 3). The one obtained at $\langle Q \rangle = 54$ MeV is compared with data taken from ref. [22] (dotted line) and ref. [6] (dashed line) and good agreement is observed. The cross section as given in [22] exceeds the one measured at PSI by the factor 1.29. The authors of ref. [6] explain this discrepancy with a possible underestimation of the mean neutron energy in the older experiment. That measurement had been carried out over a broad neutron energy range and the mean energy had been deduced from a maximum likelihood fit. In the present comparison the data of [22] have been rescaled to match the PSI cross section. For the sake of completeness we additionally give in Table 4 the numerical values of the differential π^- cross sections. In passing we like to add that the corresponding ones given in ref. [6] (Table 3 and Fig. 11) are not consistent with the absolute cross section data presented in their Table 4, but are too low by the factor $2\pi/10$ due to an error in binning the data [23].

Table 3: *Expansion coefficients of the Legendre polynomial fits to the π angular distributions.*

$\langle Q \rangle / \text{MeV}$	a_1	a_2
10	0.62 ± 0.21	0.35 ± 0.14
26	0.88 ± 0.21	0.63 ± 0.28
40	0.81 ± 0.11	0.59 ± 0.14
54	0.65 ± 0.07	0.63 ± 0.07
68	0.50 ± 0.08	0.58 ± 0.06
82	0.36 ± 0.07	0.40 ± 0.06

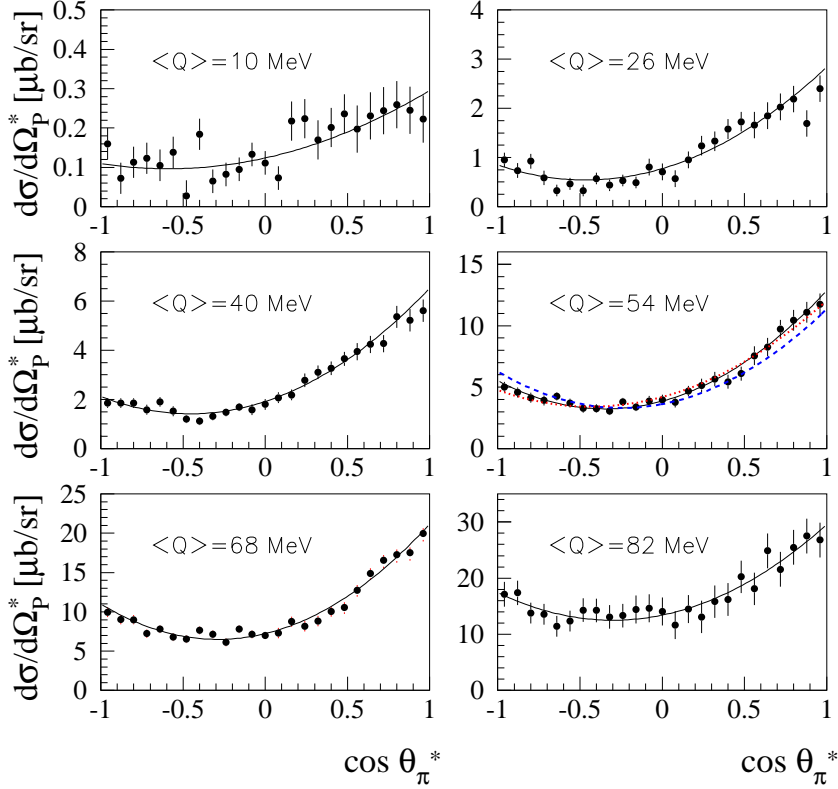


Figure 7: (Color online) Angular distributions of the pions for selected excess energies $\langle Q \rangle$ together with results of Legendre polynomial fits. At $\langle Q \rangle = 54$ MeV, the pion angular distributions as found by Daum et al. [6] and Handler [22] are also shown as a dashed (blue) and a dotted (red) curve, respectively.

3.2 Dalitz plots and invariant mass distributions

Dalitz plots and M_{pp} invariant mass distributions of acceptance corrected and kinematically fitted $pp\pi^-$ events are presented in Figs. 8 and 9 together with statistical errors in the latter figure. In each case four Q bins 2 MeV wide were chosen, the center values are indicated in each frame. The kinematical limits of the Dalitz plots given by the solid lines were calculated for these values; due to the rapidly growing phase space some data extend over these border lines. Here the size of the squares is a measure of the count rate. Each plot is almost uniformly covered with the exception of the area in the upper left corner where strong FSI effects between the reaction protons were expected. Also some lowering in yield is observed in the opposite corner which we attribute to the asymmetries found in the pion angular distributions. No enhancements due to the Δ resonance are visible.

Table 4: *Differential cross sections in $\mu\text{b}/\text{sr}$ of the pion angular distributions at six excess energies Q .*

$\cos \theta_\pi^*$	10 MeV	26 MeV	40 MeV	54 MeV	68 MeV	82 MeV
-0.96	0.160±0.041	0.95±0.15	1.85±0.21	5.01±0.45	9.95±0.61	17.1±2.3
-0.88	0.072±0.039	0.73±0.13	1.85±0.20	4.57±0.42	9.01±0.60	17.4±2.2
-0.80	0.113±0.041	0.92±0.14	1.85±0.20	4.14±0.42	9.00±0.58	13.8±1.9
-0.72	0.123±0.038	0.58±0.13	1.58±0.18	3.92±0.41	7.23±0.55	13.6±1.8
-0.64	0.105±0.042	0.32±0.12	1.90±0.19	4.24±0.37	7.82±0.54	11.4±1.5
-0.56	0.138±0.037	0.46±0.11	1.52±0.18	3.71±0.37	6.80±0.52	12.4±1.5
-0.48	0.027±0.038	0.32±0.11	1.20±0.16	3.27±0.35	6.55±0.53	14.3±1.8
-0.40	0.184±0.036	0.57±0.11	1.12±0.16	3.26±0.34	7.65±0.52	14.3±1.7
-0.32	0.065±0.034	0.43±0.12	1.31±0.15	3.05±0.33	7.14±0.50	13.1±1.9
-0.24	0.082±0.031	0.53±0.13	1.47±0.14	3.81±0.35	6.12±0.50	13.3±2.0
-0.16	0.095±0.032	0.49±0.13	1.69±0.16	3.37±0.36	7.82±0.52	14.4±2.4
-0.08	0.133±0.029	0.80±0.15	1.58±0.17	3.86±0.38	7.14±0.53	14.6±2.4
0.0	0.111±0.028	0.70±0.17	1.80±0.19	3.97±0.40	6.97±0.52	14.0±2.3
0.08	0.073±0.033	0.57±0.16	2.07±0.21	3.76±0.39	7.31±0.58	11.7±2.2
0.16	0.218±0.038	0.95±0.18	2.18±0.23	4.68±0.43	8.76±0.61	14.5±2.5
0.24	0.224±0.042	1.23±0.20	2.78±0.26	5.12±0.48	8.16±0.64	13.1±2.3
0.32	0.170±0.047	1.33±0.21	3.10±0.29	5.66±0.50	8.84±0.66	15.8±2.6
0.40	0.201±0.051	1.57±0.23	3.27±0.29	5.44±0.53	10.03±0.71	16.2±2.9
0.48	0.236±0.052	1.72±0.25	3.65±0.32	6.10±0.58	10.55±0.75	20.2±2.8
0.56	0.197±0.058	1.66±0.25	3.95±0.35	7.56±0.63	12.76±0.91	18.1±3.1
0.64	0.231±0.060	1.85±0.24	4.24±0.34	8.27±0.74	14.88±1.12	24.9±3.1
0.72	0.244±0.061	2.03±0.28	4.27±0.38	9.74±0.88	16.58±1.18	21.6±3.2
0.80	0.259±0.061	2.19±0.29	5.36±0.41	10.45±0.88	17.26±1.22	25.5±3.4
0.88	0.245±0.063	1.69±0.27	5.22±0.43	11.10±0.92	17.52±1.28	27.5±3.3
0.96	0.223±0.064	2.40±0.30	5.61±0.46	11.76±0.95	19.98±1.41	26.8±3.5

The $d\sigma/dM_{pp}$ invariant mass distributions shown in Fig. 9 were plotted on a linear M_{pp} scale, also given are the results obtained from our Monte Carlo simulation (solid and dashed lines). In all cases large deviations are observed between experimental and simulated data, as long

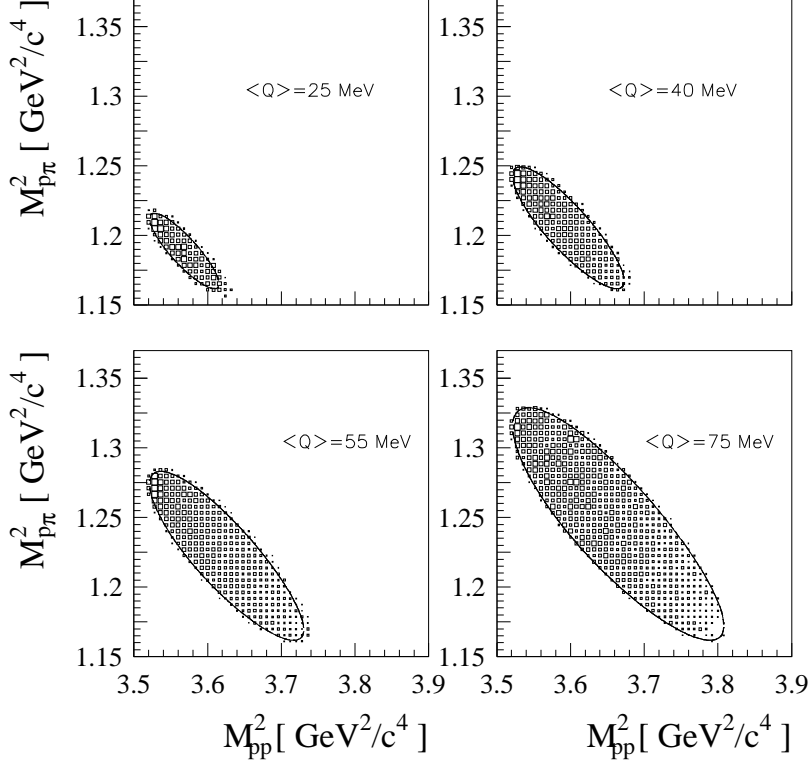


Figure 8: *Experimentally deduced Dalitz plots for the quasifree reaction $np \rightarrow pp\pi^-$ at four 2 MeV wide Q bins. The solid lines denote the kinematical limits.*

as purely phase space distributed events were considered (dashed lines). Incorporating FSI effects into our MC simulations by using the formalism of Watson [24] and Migdal [25] which was later refined by Morton [26] the distributions given by the solid lines were found. We calculated additional weight factors w_{fsi} given in a simplified form as

$$w_{fsi} = 1 + f_{pp} \cdot C^2 \cdot [C^4 \cdot T_{pp}^{CM} + \frac{(\hbar c)^2}{m_p c^2} \left(\frac{m_p c^2}{2(\hbar c)^2} r_0 \cdot T_{pp}^{CM} - \frac{1}{a_0} \right)^2]^{-1}, \quad (7)$$

where T_{pp}^{CM} denotes the pp center of mass kinetic energy $T_{pp}^{CM} = (M_{pp} - 2m_p) c^2$ and C^2 the Coulomb penetration factor

$$C^2 = \frac{2\pi \cdot \gamma_p}{e^{2\pi\gamma_p} - 1} \quad (8)$$

with $\gamma_p = \frac{\alpha \cdot \mu_{pp} \cdot c}{p_{pp}}$. Here α is the fine structure constant, $p_{pp} = \sqrt{2\mu_{pp}T_{pp}^{CM}}$ and μ_{pp} is the reduced mass of the pp -system. The strength factor f_{pp} is a measure of the contributing

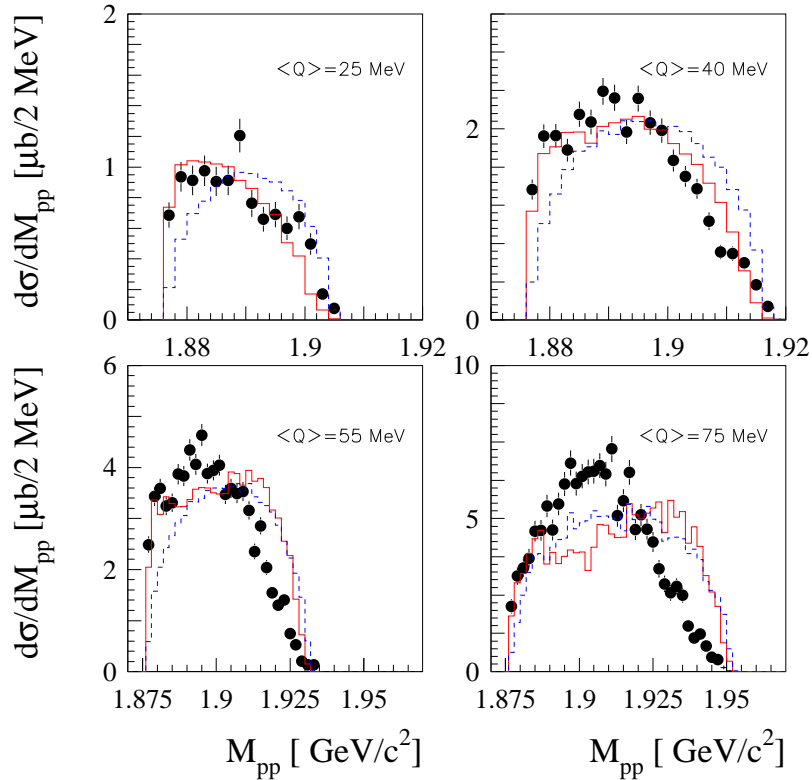


Figure 9: (Color online) Proton-proton invariant mass distributions obtained at four Q bins together with data from our Monte Carlo simulation. The dashed (blue) lines denote the results as found for phase space distributed events, the solid (red) curves give the ones where FSI effects with standard values for scattering length and effective range have additionally been included (see text).

S_s and S_p partial waves and is adjusted for each Q interval. From literature we took the standard values $a_0 = -7.83$ fm and $r_0 = 2.8$ fm [27] as input parameters for the scattering length and effective range, respectively, for the two protons in the 1S_0 state. The agreement for the two lowest Q bins, where the relative weight of the “diproton” 1S_0 -state is high, is very good. In case of the two higher bins this simple ansatz, however, only succeeds in reproducing the rise at $M_{pp} = 2m_p$.

3.3 The isoscalar cross section

Using equation (1) the isoscalar cross section σ_{01} can be obtained from the measured cross sections for the $pp \rightarrow pp\pi^0$ and the $np \rightarrow pp\pi^-$ reactions. The isospin $I=0$ partial waves of type Sp (${}^3S_1 \rightarrow {}^1S_0p_1$ and ${}^3D_1 \rightarrow {}^1S_0p_1$) which are forbidden in the $pp \rightarrow pp\pi^0$ reaction due to the Pauli principle are generally believed [2,6,10,11] to dominate σ_{01} in the threshold region. In the np reaction they interfere with the isospin $I=1$ wave ${}^3P_0 \rightarrow {}^1S_0s_0$ and thus are responsible for the strong asymmetries in the π^- angular distributions at very low excess energies. In the literature one finds a vast amount of data for both reactions and, as has been shown [6], the extracted σ_{01} shows the expected η^4 dependence [3], at least for $\eta > 0.5$ ($Q > 17\text{MeV}$). We contend that the deviations quoted for smaller η values are the result of wrong cross section data. As can be seen from (1), in order to obtain a finite σ_{01} the np cross section must at least be half as large as the one for the pp reaction. For $\eta=0.34$ σ_{np} is given as $1.43\ \mu\text{b}$ [6]. Recently our group at COSY reported new data for the $pp \rightarrow pp\pi^0$ reaction which exceeded the published ones from IUFC [28] and CELSIUS [29] by roughly 50%, the discrepancy could be shown to originate from an underestimation of the pp final-state interaction [30]. We found a cross section $\sigma_{pp} = 3.72 \pm 0.3\ \mu\text{b}$ at $\eta=0.35$ which is 2.6 times larger than σ_{np} and as such would leave no room for σ_{01} . This, however, is in contradiction to the asymmetries observed for the π^- angular distributions, which are only possible with interfering Ss and Sp partial waves. In addition to assuming a wrong cross section measurement one should also consider a wrong beam energy determination. The uncertainty in neutron energy at the NA2 beam facility at PSI is given as 3 MeV (σ) for $E_n = 287\text{MeV}$ [6]. An error in quoted beam energy of this size could possibly explain the observed deviations in the very close to threshold region where the cross section of almost any reaction rises dramatically.

3.4 Summary

With a deuteron beam at $1.85\text{GeV}/c$ impinging on a liquid hydrogen target the quasi-free $np \rightarrow pp\pi^-$ reaction was studied for excess energies Q up to 90 MeV. The data were analyzed in the framework of the spectator model where the proton is assumed to be an unaffected spectator staying on-shell throughout the reaction. Tagging the spectator proton in the forward scintillator hodoscope of our COSY-TOF spectrometer allowed to determine such parameters as effective mass and momentum of the off-shell neutron at the time of the reaction. We have measured angular distributions and invariant mass distributions of the

reaction products and have set up Dalitz plots for several Q bins distributed evenly over the whole excess energy range. The data were compared to results derived from Monte Carlo simulations and to data taken from the literature. In general good agreement was found, the large asymmetries observed previously for the π^- angular distributions could be confirmed. Final-state interaction effects between the reaction protons were found even at the highest excess energies. The $d\sigma/dM_{pp}$ invariant mass distributions at 25 and 40 MeV which are governed by the “diproton” 1S_0 -state could be reproduced by the Monte Carlo simulations when incorporating FSI effects in the formalism of refs. [23-25] with standard values for scattering length and effective range. Sizeable d -wave contributions were observed in the angular distribution of the relative proton momentum at $Q = 82$ MeV. In view of new cross section data of the $pp \rightarrow pp\pi^0$ reaction, reported deviations of the isoscalar cross section σ_{01} from an η^4 dependence [6] were explained as stemming most probably from small errors in beam energy.

Acknowledgements

The big efforts of the COSY crew in delivering a low-emittance deuteron beam is gratefully acknowledged. Helpful discussions with C. Hanhart, H. Lacker, P. Moskal and C. Wilkin are very much appreciated. Special thanks are due to G. Sterzenbach who as head of the workstation group provided continuous help in case of problems with the system. Financial support was granted by the German BMBF and by the FFE fund of the Forschungszentrum Jülich.

References

- [1] P. Moskal et al., Progress in Particle and Nuclear Physics **49** 1 (2002)
- [2] C. Hanhart, Phys. Reports **397**, 155 (2004)
- [3] A.H. Rosenfeld, Phys. Rev. **96**, 130 (1954)
- [4] M. Kleinschmidt et al., Z. Phys. A **298**, 253 (1980)
- [5] A. Bannwarth et al., Nucl. Phys. A **567**, 761 (1994)
- [6] M. Daum et al., Eur. Phys. J. C **23**, 43 (2002)

- [7] M. Daum et al., Eur. Phys. J. C **25**, 55 (2002)
- [8] W. Thomas et al., Phys. Rev. D **24**, 1736 (1981)
- [9] M.G. Bachmann et al., Phys. Rev. C **52**, 495 (1995)
- [10] F. Duncan et al., Phys. Rev. Lett. **80**, 4390 (1998)
- [11] H. Hahn et al., Phys. Rev. Lett. **82**, 2258 (1999)
- [12] M. Abdel-Bary et al. [COSY-TOF collaboration], Eur. Phys. J. A **29**, 353 (2006)
- [13] R. Maier, Nucl. Instrum. Methods Phys. Res. A **390**, 1 (1997)
- [14] N.A. Booth et al., Phys. Rev. D **4**, 1261 (1971)
- [15] GENBOD, CERN Program Library Long Write-up W515 (1993)
- [16] S. Häggström, Thesis, University of Uppsala *Acta Universitatis Upsaliensis 13* (1997)
- [17] M. Lacombe et al., Phys. Lett. B **101**, 139 (1981) and C. Wilkin, private communication
- [18] J.C. Alder et al., Phys. Rev. C **6**, 2010 (1972)
- [19] E. Gülmez et al., Phys. Rev. C **43**, 2067 (1991)
- [20] H. Rohdjeß et al., Phys. Rev. C **57**, 2111 (1998)
- [21] E. Chiavassa et al., Phys. Lett. B **337**, 192 (1994)
- [22] R. Handler, Phys. Rev. **138**, B1230 (1965) and references therein
- [23] H. Lacker, Erratum to Eur. Phys. J. C (in print) and private communication
- [24] K.M. Watson, Phys. Rev. **88**, 1163 (1952)
- [25] A.B. Migdal, Sov. Phys. JETP **1**, 2 (1955)
- [26] B.J. Morton et al., Phys. Rev. **169**, 825 (1968)
- [27] H.P. Noyes, Annu. Rev. Nucl. Sci. **22**, 465 (1972)
- [28] H.O. Meyer et al., Nucl. Phys. A **539**, 633 (1992)
- [29] A. Bondar et al., Phys. Lett. B **356**, 8 (1995)
- [30] S. Abd El-Samad et al. [COSY-TOF collaboration], Eur. Phys. J. A **17**, 595 (2003)